Int J Adv Manuf Technol (2016) 83:133–144
DOI 10.1007/s00170-015-7483-6

ORIGINAL ARTICLE

Relationships of tool wear characteristics to cutting mechanics, chip formation, and surface quality in ultra-precision fly cutting

Guoqing Zhang[1,2] · **Suet To**[2,3] · **Shaojian Zhang**[2]

Received: 11 February 2015 / Accepted: 22 June 2015 / Published online: 21 July 2015

Abstract Although the occurrence of tool wear can affect cutting forces, cutting chip morphologies, and machined surface quality in ultra-precision fly cutting (UPFC), there has been no research in this area due to the complex cutting mechanism of UPFC. The theoretical and experimental research described in this paper was therefore conducted to explore tool wear characteristics in UPFC and their relationship to cutting forces, cutting chip morphologies, and machined surface quality. Results from the study reveal that tool wear characteristics in UPFC include cutting edge fractures, workpiece material welding, wear land formation, sub-wear land formation, and micro-grooves. The cutting edge fractures lead to the formation of ridges on both the cutting chips and machined surface; the material welding increases the thrust force, crushes cutting chips, and deteriorates the machined surface quality; and the formation of wear land on the cutting edge makes the machined surface burred and fuzzy, and the micro-grooves leave some traces on the machined surface. By analyzing the captured cutting force, it is found that the progress of tool wear in UPFC can increase the cutting force and its power spectral density at the natural frequency of the dynamometer. Findings from the research provide rich insight into the relationships of tool wear characteristics to cutting forces, chip formation, and machined surface quality in intermittent cutting processes.

Keywords Tool wear characteristics · Chip morphology · Cutting force · Surface quality · Ultra-precision fly cutting

✉ Suet To
sandy.to@polyu.edu.hk

[1] College of Mechatronics and Control Engineering, Shenzhen University, Shenzhen 518060, People's Republic of China

[2] State Key Laboratory of Ultra-precision Machining Technology, Department of Industrial and Systems Engineering, The Hong Kong Polytechnic University, Kowloon, Hong Kong, People's Republic of China

[3] Shenzhen Research Institute of the Hong Kong Polytechnic University, Shenzhen, People's Republic of China

Nomenclature

s_w	Swing distance
s_t	Step distance
l	Length of the rectangular machined plane
w	Width of the rectangular machined plane
θ	Rotation angle
r	Tool edge radius
R	Tool nose radius
H	The Vicker hardness of workpiece materials
E	The elastic modulus of workpiece materials
δ	Clearance angle of diamond tools
F_x, F_y, F_z	Cutting force components in x, y, and z directions
F_t, F_r, F_s	Cutting force components in t, r, and s directions
F_{tr}	Force component generated by material springback
σ_{t}	Rebound stress imposed on the flank face of diamond tools
k_1, k_2, K	Constants
s_{p}	Value of material springback
W_{f}	Tool–workpiece contact width on the flank face

W	Width of the wear land
f_s	Sampling frequency
l_f	Average length of contact area in the step direction
$\overline{x}$	Mean value of the measured peak-to-valley roughness
x_i	Peak-to-valley roughness in a tool imprint
m	Number of tool imprints for roughness evaluation
u_i	Roughness residuals between a measured value and a mean value
σ	Standard deviation of measured roughness

1 Introduction

The study of tool wear is an essential topic in the ultra-precision machining field since cutting tools are directly involved in forming the desired surface topography. In the surface forming process, the tool profile is directly imprinted on the machined surface so that the wear of the cutting tool affects the machined surface quality. Tool wear is an inevitable phenomenon during the metal cutting process; the contact stresses, relative sliding velocity, and cutting temperature during the cutting strongly affect tool wear on the tool–chip and tool–workpiece interfaces (i.e., tool flank wear and crater wear). These process variables depend on tool and workpiece materials, tool geometry and coatings, cutting conditions, and use of a coolant for the given application [1]. Therefore, tool wear characteristics are different in different cutting processes. For example, Liu et al. (2002) explored the wear performances of different kinds of cutting tools as milling different materials and found that the type of tool wear varied according to the combination of cutting tool and workpiece material [2]. Jawaid et al. (1999) conducted research on tool wear characteristics in the turning of titanium alloy Ti-6246 and concluded that abrasion wear mechanisms dominated the wear type at the flank face and tool nose [3]. Luo et al. (1999) studied the wear behavior of cubic boron nitride (CBN) and ceramic tools in the turning of AISI 4340 hardened alloy steels; they found that the main wear mechanism for the CBN tool was the abrasion of the binder material by the hard carbide particles of the workpiece, and for the ceramic tools was adhesive wear and abrasive wear [4]. Zhang et al. (2011) found a special kind of wear pattern—periodical groove wear on the flank face of cutting tools in diamond turning of reaction-bonded silicon carbide [5]. Sharif Uddin et al. (2004) investigated the tool wear characteristics of single-point diamond tools in nano-scale ductile cutting of silicon and found that gradual wear occurred mainly on the flank face while smooth wear happened on the rake face of the tool [6]. Wadaa et al. (1980) explored the tool wear characteristics in the case of cutting aluminum alloy and observed a smooth and flat wear land on each of the rake face and flank face [7].

Moreover, the tool wear effects on surface finish, cutting chip morphologies, and even cutting forces are also work material dependent. For example, Bakkal et al. (2004) reported that tool wear features, including the welding of chip on the tool tip and chipping of the PcBN tool edge, were the predominant tool wear types in turning of bulk metallic glass (BMG) [8]. However, due to the effect of BMG melting during the cutting, the roughness of machined BMG surfaces is generally better than the work materials of aluminum 6061-T6 and AISI 304. Jia and Zhou (2012) detected the wear behavior of rake face and flank face of cutting tools, the corresponding surface features, and the material compositions of flank wear area in the diamond cutting of glass [9]. They found that the flank wear is characterized by micro-grooves while the tool wear in the rake face is predominated by smooth craters; with the tool wear progress, the surface roughness begins to increase rapidly as the cutting mode changes from ductile to brittle. Pavela et al. (2005) focused on the influence of tool wear on surface finish in interrupted and continuous hard turning, and confirmed that the negativity of the flank wear profile is replicated on the machined surface; also, they observed a strong correlation between evolution of notch wear and that of the surface finish [10]. In addition to machined surface quality, tool wear also has some effects on the cutting chip morphologies and cutting force. Nastanka and Orodja (2012) found that the degree of change in tool wear directly impacts the chip form and the type of segmentation, and that cutting parameters also affect tool wear patterns during the metal cutting process [11]. Depending upon the cutting parameters, Meena and Mansori (2013) observed different modes of tool failure, including crater wear, flank wear, chipping, breakage, and built-up edge [12]. Katuku et al. (2009) carried out a group of experimental studies of wear, cutting forces, and chip characteristics when dry turning ASTM grade 2 austempered ductile iron (ADI) with PcBN cutting tools [13]. They found that cutting speeds are predominant to the tool wear modes while abrasion wear and thermally activated wear were the main wear mechanisms. Huang and Liang (2005) addressed an oblique chip formation force model through a mechanistic force model considering the effect of tool wear. The model-predicted forces were proved by experimental results in the turning [14]. As is discussed above, the research on tool wear characteristics and their relations to cutting forces, cutting chip morphologies, and surface finish has been found in conventional cutting, high-speed machining, single-point diamond turning, and micro-milling process; however, relative little research was found on the ultra-precision fly cutting (UPFC) process since it is a complex cutting process.

The UPFC process is a typical discontinuous cutting process whereby the diamond tool rotates across the spindle axis with high speed, cutting into and out of the workpiece surface intermittently; in every rotary cut, a crater is formed while the

piece and pieces of crater cutting generate the surface structure [15]. The intermittent cutting property of UPFC makes its tool wear characteristics different from other cutting processes [16]; there have been few studies of the actual characteristics of tool wear in the UPFC process. One of the reasons for this may be that diamond tools are commonly employed to realize the UPFC cutting process and, as Zuiker et al. (1995) pointed out, the extreme hardness and low friction coefficient of diamond tools delay the occurrence of tool wear [17]. Another reason could be, as Song et al. (2009) contended, that the discontinuous cutting mechanism of UPFC reduces contact time between the diamond tool and workpiece, which allows for superior heat dispersion to suppress the occurrence of tool wear [18]. Yin et al. (2009) conducted the most comprehensive research into tool wear characteristics in UPFC to date [19], but while they identified the characteristics as fractures or micro-chipping due to effects of impacts during the UPFC process, they neglected to study the effects of tool wear on the machined surface quality. Zhang et al. (2014) proposed a novel tool wear measurement method based on the relationship between tool fractures and the structures formed on the surface of the cutting chips [20]. Their further study explored the relationship between tool flank wear and cutting chip morphologies and found that cutting chips truncated at a comparable thickness with the width of wear land [21]. However, studies of tool wear characteristics at different tool wear stages and their effects on machined surface quality in UPFC have not been conducted before.

This research therefore focused on exploring tool wear characteristics and their relationship with cutting forces, cutting chips, and machined surface finish in UPFC. Through a group of cutting experiments, it is found that tool wear characteristics in UPFC include cutting edge fractures, workpiece material welding, wear land formation, sub-wear land formation, and micro-grooves. The study contributes to an understanding of tool wear characteristics and their effects on cutting force evolution, chip formation, and surface finish changes during tool wear progress in UPFC. By using the relation between tool wear characteristics and cutting chip morphology, machined surface topography, and cutting force, this research is potentially used to monitor tool wear and its effects on machined surface quality, which can lower the cutting cost and improve the cutting efficiency.

2 Experiments

A Precitech 705G CNC ultra-precision machine (Precitech Inc., USA) was used to machine the desired surface structures for the experiments. Figure 1 shows the experimental setup. In the ultra-precision machining process, the workpiece is mounted on a rotatable table (B axis), while the diamond tool is installed on an aerostatic gas-bearing spindle holder that rotates circularly around the spindle axis. During the cutting process, the pose of the spindle can be adjusted by operating the rotatable C axis so that multiple surface structures can be machined.

In this research, the commonly used material for ultra-precision machining CuZn30 is used as workpiece material, which owns better diamond-machinable property and proper hardness. To obtain a relative larger size of cutting chips and a bigger cutting force amplitude, the cutting parameters used in this experiment are a little larger than that commonly used, the cutting parameters of which are listed in Table 1. To explore the tool wear progress, a group of desired flat cutting was conducted; the total straight cutting distance is about 5000 m. During the cutting process, cutting chips were collected and then examined by a Hitachi TM3000 scanning electron microscope (SEM). After every 1000 m of cutting, the diamond tool was taken out and inspected by the Hitachi TM3000 SEM. Meanwhile, the workpiece was dismounted and inspected by a Wyko NT 8000 microscope and an Olympus BX60 optical microscope.

During the cutting process, the cutting force was captured by a dynamometer Kistler 9256C1 mounted between the workpiece and fixture, while the fixture was directly mounted on the B axis rotary table of the Freeform 705G ultra-precision machine. In the measurement process, the dynamometer Kistler 9256C1 captured cutting force signals first and amplified them by a Kistler 5080A charge amplifier, and then a Kistler 5697A2 DAQ System was used to convert the amplified analog signals to digital signals at a sampling frequency of 300,000 Hz so that the DynoWare software could read the data. The signals also could be output by DynoWare and analyzed using Matlab software. The captured cutting forces at different cutting distances were compared and then analyzed by power spectrum analysis.

In UPFC, the straight cutting distance is used, which merely considers the total length of tool trajectory while neglecting the overlap during the cutting process. As illustrated in Fig. 2, if the workpiece has a rectangular plane with a length of l and width of w, the straight cutting distance for a complete plane cutting can be calculated as

$$\frac{lw}{s_t} \tag{1}$$

where s_t is the step distance. Therefore, for the rectangular workpiece surface used in this experiment with a length of 50 mm and a width of 25 mm, the step distance is 0.025 mm; the cutting distance over a complete plane cutting is calculated as 50 m based on Eq. (1). In this experiment, each workpiece has 20 layers of plane cutting; thus, five workpiece produce a total of 5000 m of straight cutting distance.

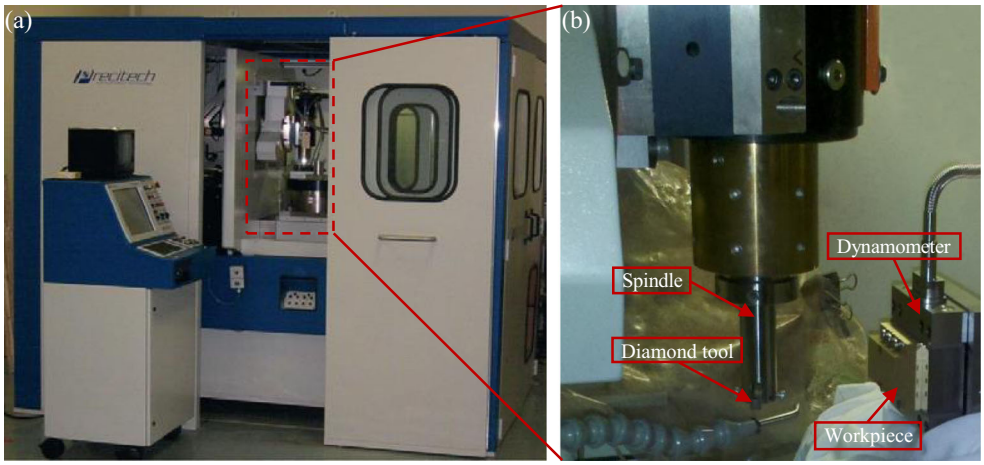

Fig. 1 **a**, **b** Freeform 705G ultra-precision fly cutting machine (Precitech Inc., USA) and the experimental setup

3 Results and discussion

3.1 Tool wear characteristics

Figure 3 shows the tool wear characteristics at different cutting distances. It indicates that after cutting about 1000 m, some fractures occurred on the cutting edge, as shown in Fig. 3a, the distribution of these fractures on the cutting edges has no order and follows statistical laws. After cutting about 2000 m, some workpiece material was found welded on the rake face of the diamond tool and the small fractures had disappeared so that only some relatively larger flattened fractures could be inspected (see Fig. 3b). In addition, a rounded cutting edge is formed. The small fractures were probably flattened or rounded during the UPFC process.

After cutting about 4000 m, it is found that the welded material on the rake face of the diamond tool is smoother, which is caused by the fiction between the rake face of the diamond tool and cutting chips (see Fig. 3c). It can also be seen from Fig. 3c that a wear land has formed with a width of about 1 μm. This wear land incorporates small fractures and relatively large fractures that have been flattened, and the craters that existed in Fig. 3b are flattened and hard to distinguish. Figure 3d shows diamond tool figures after cutting about 5000 m. It reveals that a sub-wear land with a width of about 0.5 μm is formed on the upper edge of the wear land. The formation of the sub-wear land may re-sharpen the cutting edge due to its relatively larger wear land angle and thereby improve the cutting performance.

After 5000 m of flat cutting, it is found that several micro-grooves occurred on the flank face of the cutting tool. The micro-grooves have a meandering trajectory almost parallel to the cutting direction, which originated in several micro-chips on the bottom edge of the wear land, as shown in Fig. 4.

Table 1 Cutting conditions in flat cutting

Cutting parameters	
Tool type	APEX insert diamond tool
Rake angle	−2.5°
Clearance angle	15°
Tool radius	0.631 mm
Swing distance	28.35 mm
Feed rate	200 mm/min
Step distance	0.025 mm
Spindle speed	4500 rpm
Depth of cut	0.03 mm
Cutting strategy	Horizontal cutting
Cutting environment	Lubricant on

3.2 Effect of tool wear on cutting chips

As the removal material during the cutting process, cutting chips have a close relationship with tool wear characteristics. Figure 5 shows the cutting chip morphologies formed from different tool wear characteristics. Figure 5a shows the cutting chip morphology at the cutting distance of 1000 m; it is found a feather-like structure is formed at the tool entry side of cutting chips, which is formed by a fresh cutting edge. Also some "ridges" are found which are along the cutting direction; these

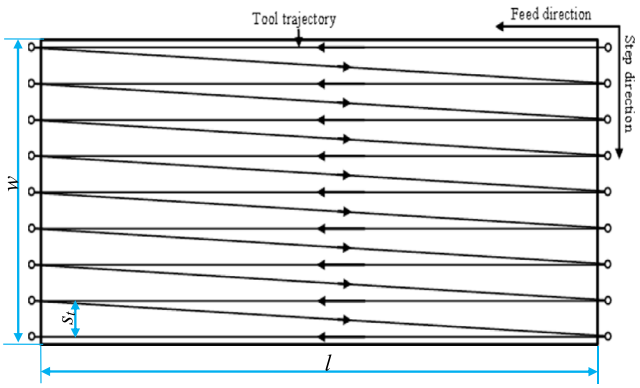

Fig. 2 Schematic illustration of straight cutting distance

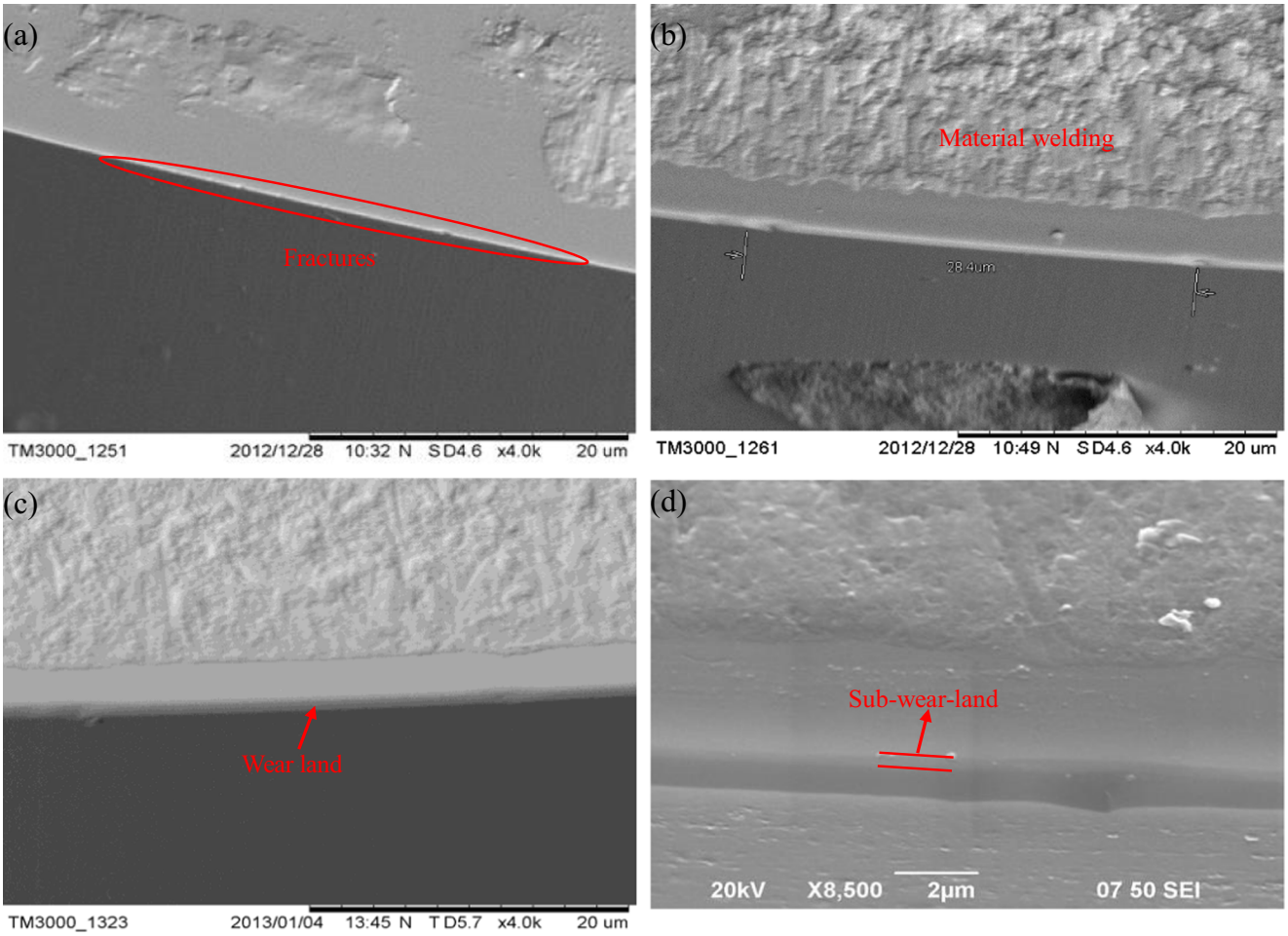

Fig. 3 Diamond tool wear characteristics at the cutting distance of **a** 1000 m, **b** 2000 m, **c** 4000 m, and **d** 5000 m

ridges are formed by the imprint of the tool fractures. After 2000 m of flat cutting, as the workpiece material welds on to the rake face of the cutting tool, cutting chips are crushed at their tool entry side due to the increase of friction on the interface between the cutting tool and cutting chips, as shown in Fig. 5b. After 4000 m of flat cutting, as a wear land forms on the cutting edge, cutting chips appear as a shutter-like structure at its tool entry side under the effect of minimum cutting depth, as shown in Fig. 5c. After the 5000-m flat cutting, as micro-grooves form on the flank face of a cutting tool, some pin-like structures are formed at the tool entry side of the cutting chip, as shown in Fig. 5d.

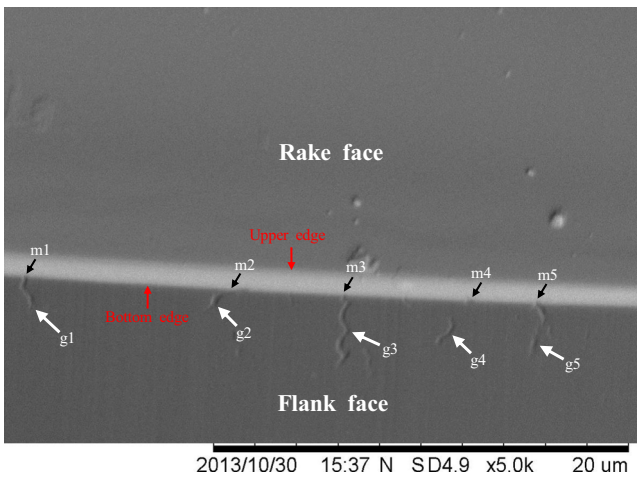

Fig. 4 Micro-grooves occurring on the flank face of the cutting tool

3.3 Effect of tool wear on cutting forces

In the UPFC process, the analysis of cutting force is important because it is closely related to diamond tool wear. The captured original cutting force signals are shown in Fig. 6. The Kistler 9256C1 dynamometer owns three channels; therefore, it can capture cutting force signals in x, y, and z directions.

Because cutting force in the thrust direction is more sensitive to diamond tool wear, it was analyzed in this research to help identify tool wear characteristics. The cutting force components imposed on the diamond tool in UPFC are plotted in Fig. 7. F_x, F_y, and F_z are the instantaneous force components along the feed direction, normal to the workpiece surface, and along the step direction, respectively, which are measured directly by using a dynamometer. F_r, F_t, and F_s are the instantaneous force

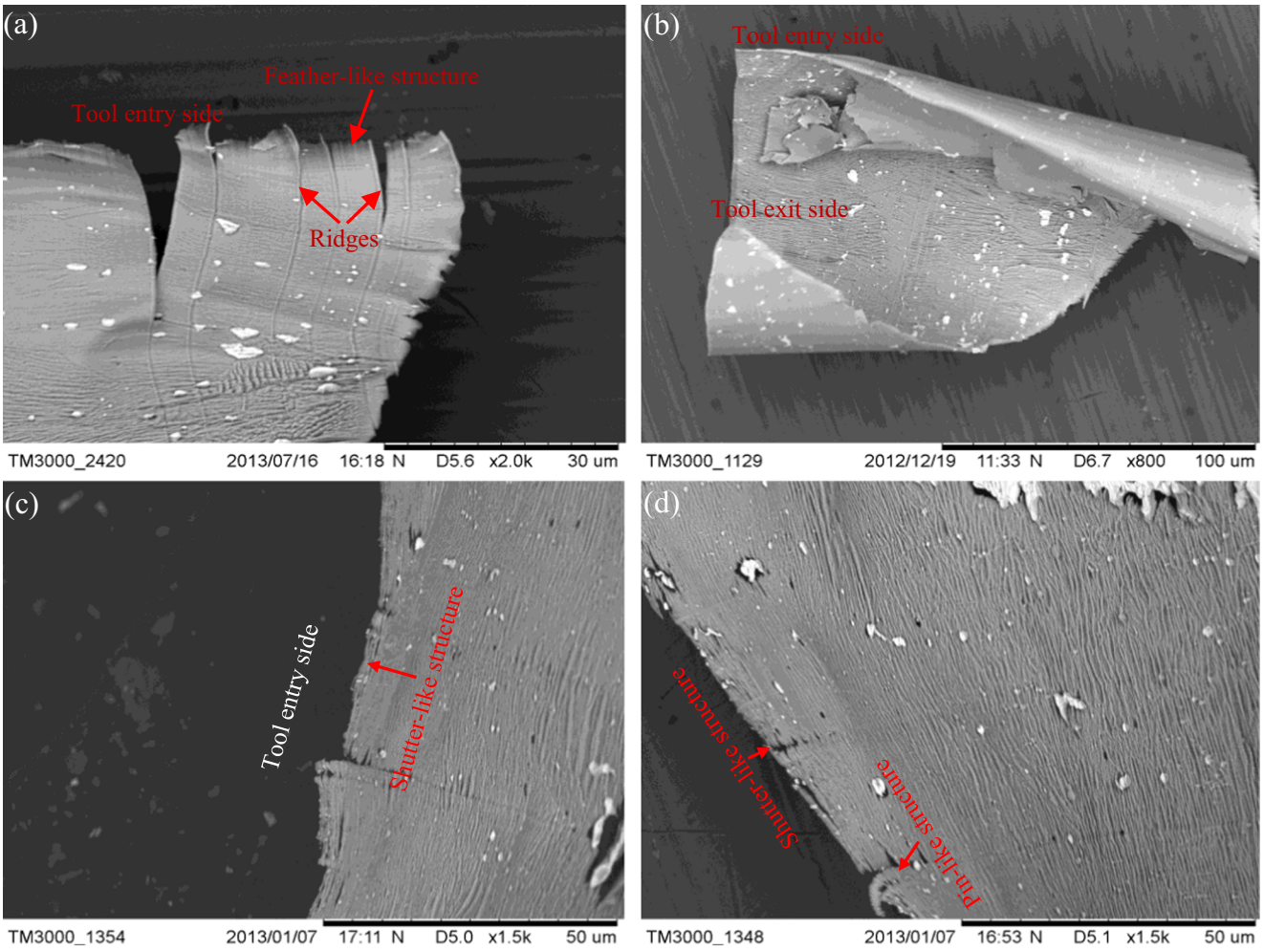

Fig. 5 Cutting chip morphologies formed at different cutting distances: **a** 1000 m, **b** 2000 m, **c** 4000 m, and **d** 5000 m

components along the cutter axis direction, along the cutting direction, and along the step direction, respectively. As the force components F_x, F_y, and F_z are obtained, the force components F_r, F_t, and F_s are merely a function of the rotation angle of the diamond tool, given by

$$\begin{aligned} F_r &= F_x \sin\theta + F_y \cos\theta \\ F_t &= F_x \cos\theta - F_y \sin\theta \\ F_s &= F_z \end{aligned} \tag{2}$$

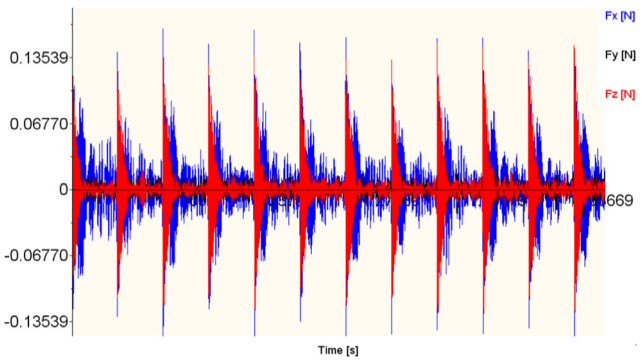

Fig. 6 Original cutting force signals

where θ is the rotation angle of the diamond tool.

Cutting force can be used to depict tool wear level. As shown in Fig. 8, the cutting forces in the thrust direction at different cutting distances were captured and compared so that the cutting force evolution with the diamond tool wear could be explored.

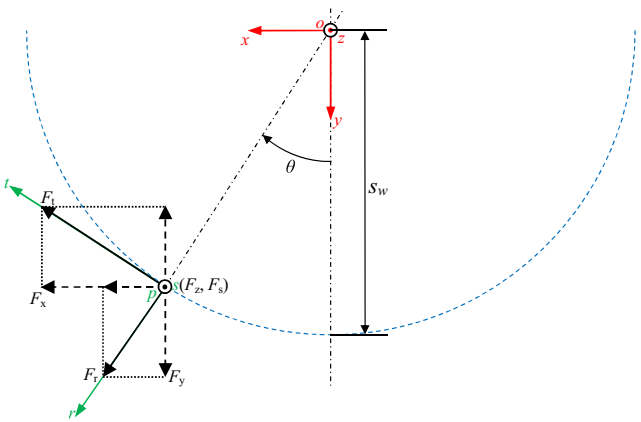

Fig. 7 Cutting force components imposed on the diamond tool

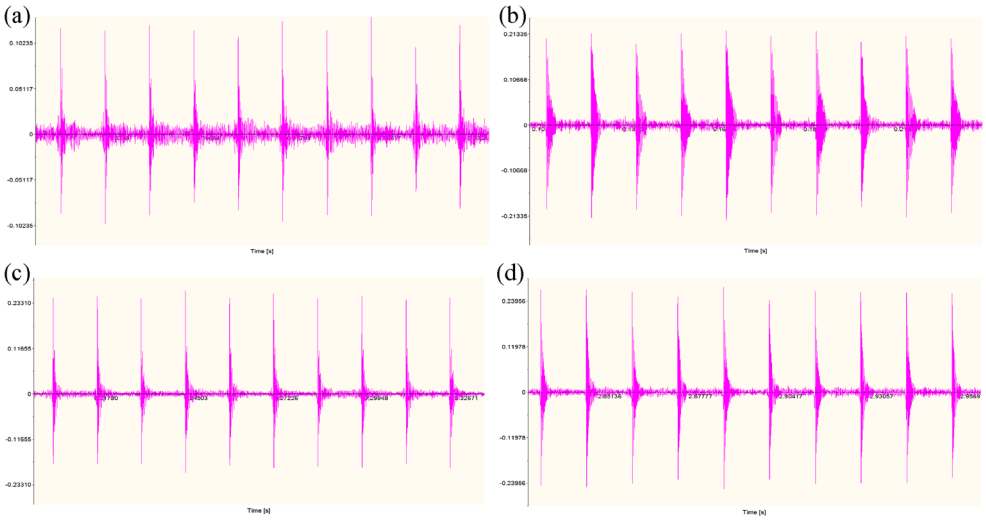

Fig. 8 Comparison of cutting force at the cutting distances of **a** 1000 m, **b** 2000 m, **c** 3000 m, and **d** 4000 m

Figure 8 reveals that the amplitude of cutting force changes from 0.125 N at the cutting distance of 1000 m to 0.205 N at the cutting distance of 2000 m, to 0.241 N at the cutting distance of 3000 m, and finally to 0.265 N at the cutting distance of 4000 m. It can be concluded that the amplitude of the cutting force increases gradually with the increase of the cutting distance. From Fig. 8, it is found that the increase of cutting force from the cutting distances of 1000 to 2000 m is relative larger than other cutting distance increases. This is due to the occurrence of material welding at the rake face of the diamond tool, which increases friction on the rake face that subsequently increases the measured cutting force in the thrust direction.

According to Arcona and Dow (1998) [22], the discontinuous contact between the cutting tool and workpiece during the UPFC process will impose cyclic cutting impact stresses and thermal impact stresses on the cutting edge of the diamond tool. With the continuance of the cutting process, the cutting conditions and stress state of the diamond tool gradually wear the diamond tool, which will increase the contact area between the diamond tool and the workpiece and enlarge the cutting force.

In UPFC, the amplitude of the cutting force in the thrust direction increases with the diamond tool wear because the cutting force in the thrust direction is mainly generated by the material springback to the flank face of the diamond tool. The flank wear of the diamond tool will increase the contact area between the diamond tool and workpiece and increase the cutting force in the thrust direction (see Fig. 8).

According to Kang et al. (2007) [23], the value of material springback is a function of the tool edge radius, the hardness, and the elastic modulus of the workpiece material, which is given by

$$s_p = k_1 rH \Big/ E \tag{3}$$

where k_1=43 is a constant, r is the tool edge radius, and H and E are the Vicker hardness and the elastic modulus of workpiece materials, respectively.

Thus, the tool–workpiece contact width W_f on the flank face can be derived as

$$W_\mathrm{f} = \frac{s_p}{\sin\delta} = \frac{k_1 rH}{E\sin\delta} \tag{4}$$

where δ is the clearance angle of the diamond tool.

For a worn tool, the total contact width is $W+W_\mathrm{f}$, as shown in Fig. 9, where W is the width of the wear land on the cutting edge of the diamond tool.

The rebound stress imposed on the flank face of the diamond tool can be expressed as [24]

$$\sigma_t = k_2 H\sqrt{s_p \Big/ r} = KH\sqrt{H \Big/ E} \tag{5}$$

where k_2=0.625 and $K = k_2\sqrt{k_1} = 4.1$ are constants.

Therefore, the force generated by material springback can be derived as

$$F_\mathrm{tr} = \sigma_t(W_\mathrm{f} + W)l_f = KHl_f\sqrt{H \Big/ E}\left(\frac{k_1 rH}{E\sin\delta} + W\right) \tag{6}$$

where l_f is the average length of the contact area along the step direction.

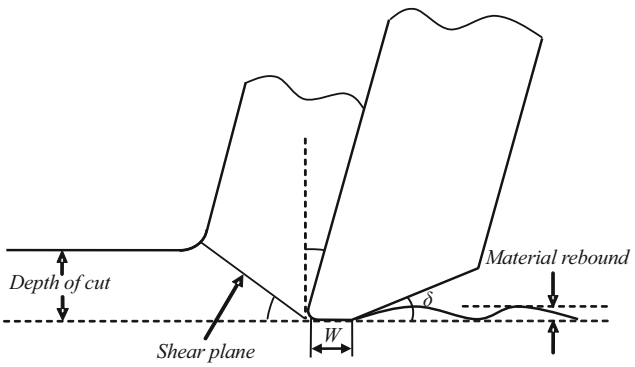

Fig. 9 Schematic illustration of the cutting process by a worn tool

Equation (6) is the formula to calculate the force generated from material springback. It is found that F_{tr} is closely related to the width of the wear land such that an increase in the width of the wear land can directly increase F_{tr}.

In UPFC, the power spectral density (PSD) of the cutting force signals can be obtained by computing its discrete Fourier transformation (DFT) through the fast Fourier transformation (FFT) algorithm, and the power spectrum of the cutting force signals can be calculated by the following formula proposed by Sze et al. (2006) [25]:

$$P(f_n) = \sum_{k=0}^{N-1} F(kl_s) e^{-2\pi i k l_s f_n} \tag{7}$$

where f_n denotes the nth frequency component of the cutting force signals, f_s is the sampling rate, and N is the number of samples in a sampling period. According to the sampling theorem, the sampling rate f_s should be at least two times as large as the highest non-zero frequency component f_{max} of the cutting force signals, i.e., $f_s \geq 2f_{max}$. In this experiment, the sampling rate is 300,000 Hz.

By using power spectrum analysis, the characteristic frequencies of cutting forces by which the diamond tool wear characteristics in UPFC can be represented were explored. Figure 10a shows the power spectral plots of cutting forces in the air cutting condition. It is found that the background power spectrum peaks mainly accumulate at three frequency bands: 0–700, 2500–3200, and 4500–5100 Hz. Figure 10b–d shows the power spectral plots of cutting force at the cutting distance of 2000, 3000, and 4000 m, respectively. It is found that the power spectrums at the frequency bands of 0–700 and 2500–3200 Hz have no significant change with the increase of cutting distance. However, the power spectrum at the frequency band of 4500–5100 Hz (the dynamometer's natural frequency) changes significantly at different cutting distances, e.g., the PSD increases from 0.2231 at the cutting distance of 2000 m to 1.844 at the cutting distance of 3000 m and to 2.831 at the cutting distance of 4000 m. This is due to the increase of cutting force that leads to a more serious vibration of the dynamometer at its natural frequency and a relatively large natural power spectrum peak. It can also be seen from Fig. 10b that the PSD is more decentralized, which is caused

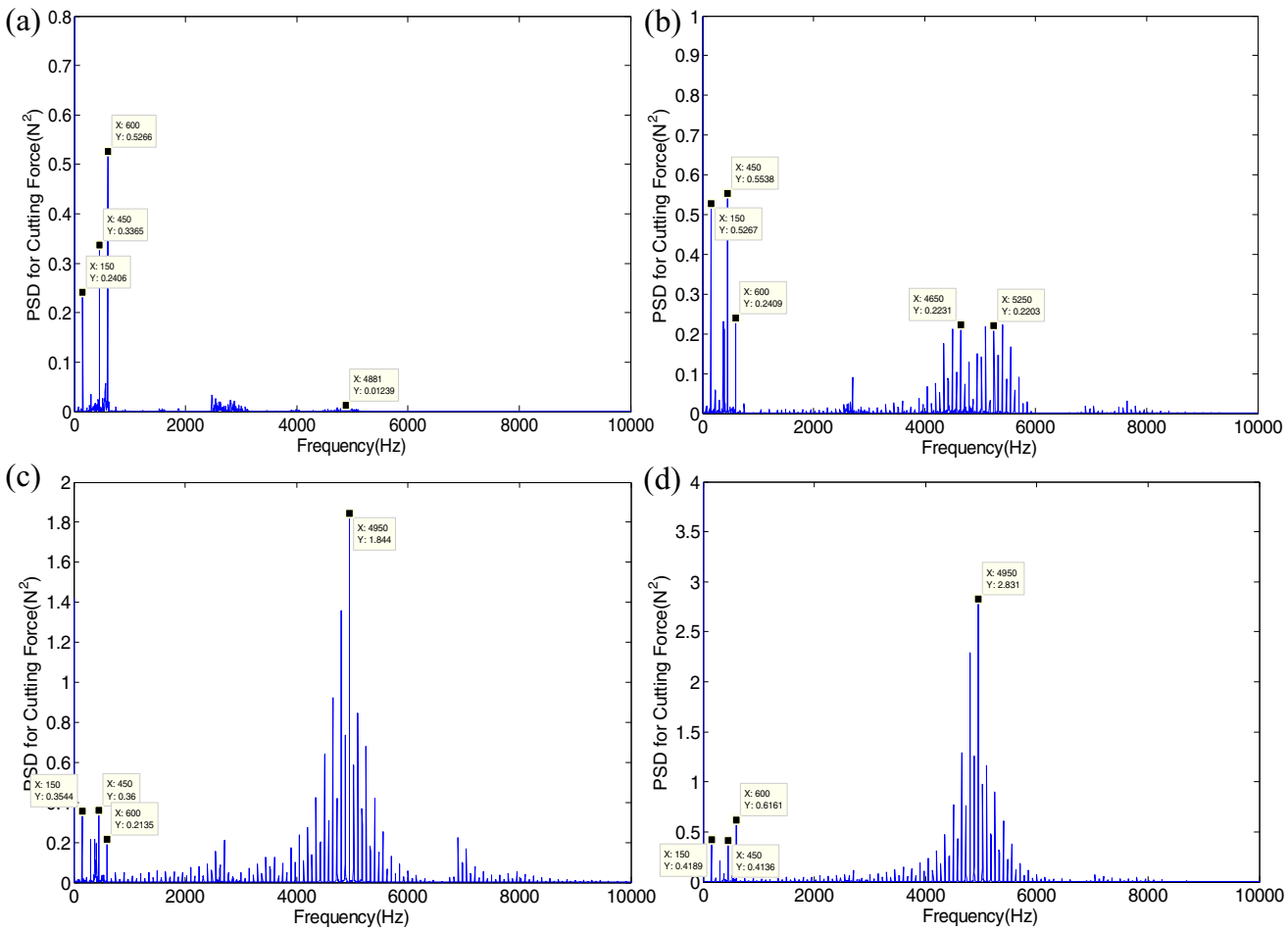

Fig. 10 Power spectrum density of the captured cutting force signals at **a** air cutting process and at the cutting distances of **b** 2000 m, **c** 3000 m, and **d** 4000 m

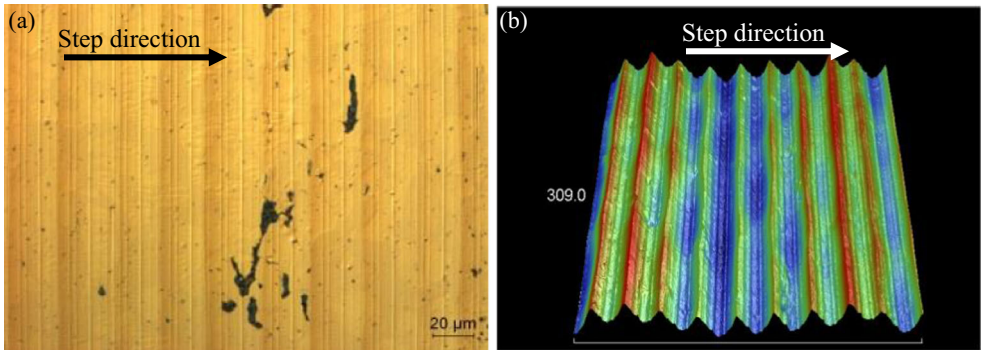

Fig. 11 **a**, **b** Surface topography formed by a cutting tool with tool fractures

by the material welding on the rake face of the diamond tool due to the friction generated from the cutting process having an unsteady damping effect. This disturbance of the natural vibration of the dynamometer will be reflected by the power spectrum plot as the dispersion of the spectrum peak.

3.4 Effects of tool wear on the machined surface quality

During the UPFC process, the imprint of the cutting edges generated the machined surface. Hence, the tool wear can directly affect the machined surface quality. The occurrence of fractures on the cutting edge of the diamond tool can lead to the generation of ridges on the machined surface, as shown in Fig. 11. The formation of ridges can deteriorate the machined surface quality and affect the optical function of machined products.

The occurrence of material welding can lead to breakage of cutting chips, and the broken cutting chips can scratch the machined surface and lead to a poor-quality surface. Figure 12 shows the machined surface topography inspected by an Olympus BX60 optical microscope and a Wyko NT8000 microscope. In Fig. 12a, it is found that the machined surface is fuzzy; the broken chips burr and deteriorate the machined surface. The poor machined surface topography can also be inspected from Fig. 12b, which shows black points due to missing data in some inspection areas because the existing burrs exceed the field depth of the Wyko NT8000 microscope. However, with the increase of cutting distance, the welded material is gradually flattened and its effect on the machined surface quality also decreases.

The occurrence of flank wear on a cutting tool also has some effects on the quality of the machined surface. With the progress of tool flank wear, a plowing effect instead of cutting occurs. The plowing is harmful since it can lead to the formation of burrs at the bottom of tool imprints. Figure 13 shows the machined surface topography at different cutting distances. It is found that at the cutting distance of 1000 m, the machined surface patterns are clear and well shaped, as shown in Fig. 13a. Figure 13b illustrates that the surface topography at the cutting distance of 3000 m is a little fuzzy due to the changing of process from cutting to plowing that caused a pile up of material. Figure 13c indicates that after 5000 m of cutting, the surface topography is extremely unclear. This is because by that time, plowing instead of cutting had become the dominant machining process resulting in a substantial buildup of material.

In addition, it is found that with the increase of cutting distance, the surface roughness R_z at the inspection area increases slightly. During the cutting process, the surface roughness suffers from the effects of multi-factors such as tool tip vibration, slide error, spindle vibration, and even material springback. These factors may make the surface roughness value different at different measurement areas.

To explore the effects of tool flank wear on machined surface roughness, the mean peak-to-valley values of the machined surface at different cutting distances were measured. As shown in Fig. 14, the mark profile of tool imprints is undulating due to the

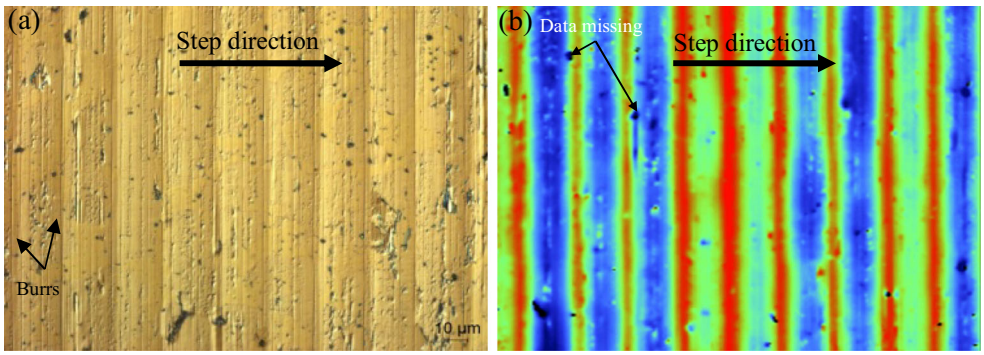

Fig. 12 **a**, **b** Surface topography formed by cutting tool material welding on the rake face

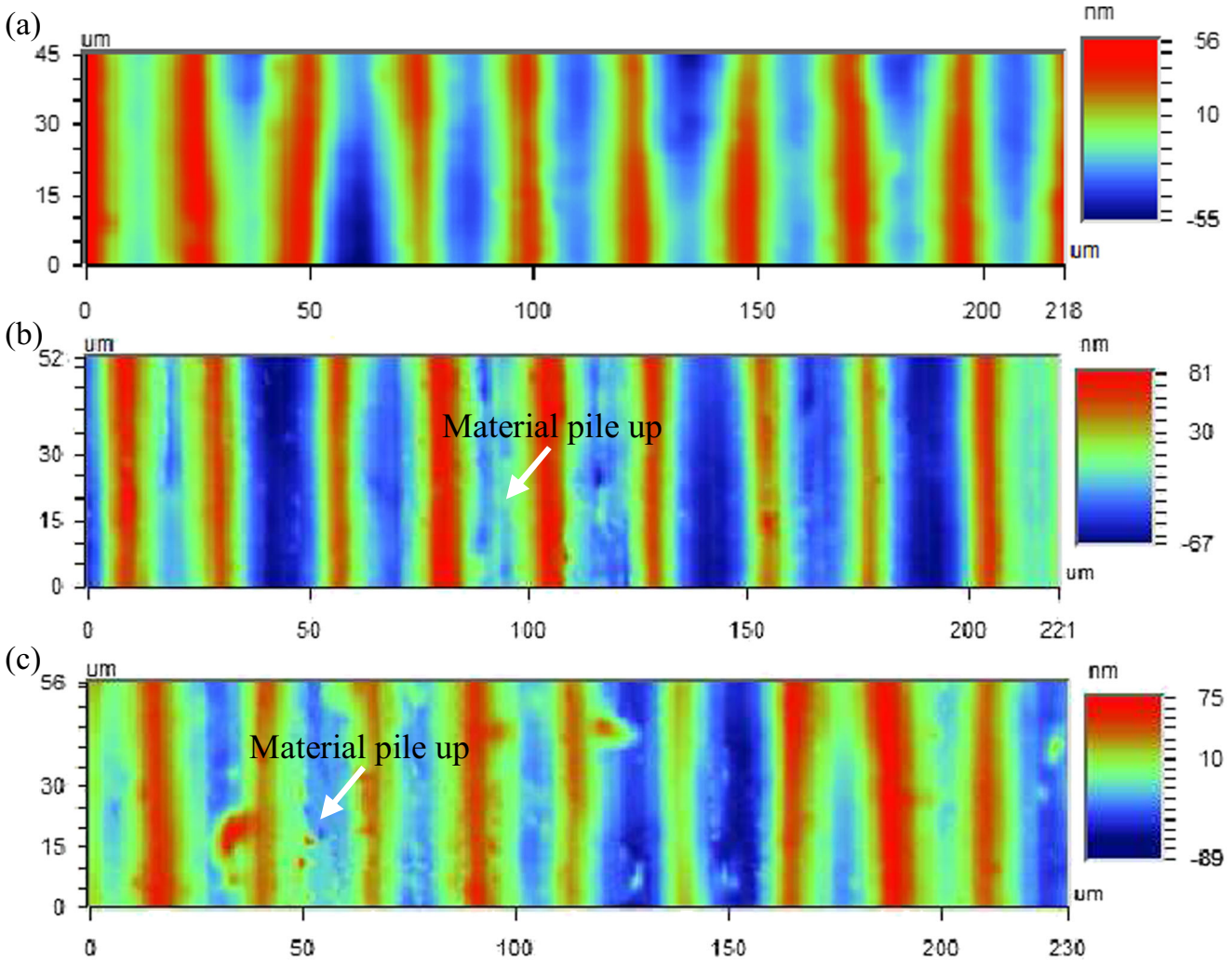

Fig. 13 Surface topography at the cutting distances of **a** 1000 m, **b** 3000 m, and **c** 5000 m. The *white arrows* are used to point out the material pile up on the machined surface

existence of surface-affecting factors. However, these factors exist at all tool wear stages, which can be subtracted and suppressed. It should be mentioned that although the plowing effect may cause burrs on the machined surface, they can be distinguished and neglected during the recording of peak-to-valley values in a tool imprint mark. In Fig. 14, p_i denotes the peak value of tool mark boundary, while u_i is the valley value of the tool mark boundary. The peak-to-valley roughness can be calculated by solving the mean value of the deviation between peaks and valleys of the tool marks.

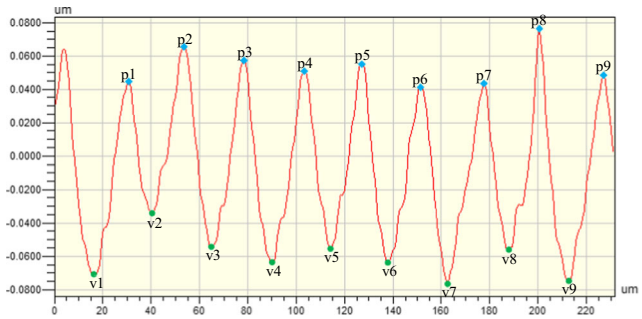

Fig. 14 Tool imprint mark profile used to identify peak-to-valley roughness

Statistical methodology is used to process the measured peak-to-valley roughness. Suppose the measured peak-to-valley values in each tool imprint are defined as $x_1, x_2, \ldots, x_m$.

The mean value of these measured peak-to-valley values can be calculated by

$$\bar{x} = (x_1 + x_2 + \cdots + x_m) \Big/ m = \sum_{1}^{m} x_i \Big/ m \tag{8}$$

Table 2 Surface roughness at different cutting distances

Cutting distance (m)	1000	2000	3000	4000	5000
Wear land width (μm)	0.24	0.61	0.61	0.74	0.86
Mean *p–v* values (nm)	123.66	123.45	124.05	124.44	125.51
Standard deviation (nm)	10.04	9.87	9.87	11.63	11.23

where x_i is the measured value of each sample, $\overline{x}$ is the mean value of the measured peak-to-valley values, and m is the total amount of samples.

The residuals between the measured value of x_i and the mean value of $\overline{x}$ can be calculated by

$$u_i = x_i - \overline{x} \tag{9}$$

According to the Bessel formula, the estimation of the standard deviation can be solved by

$$\sigma = \sqrt{\frac{u_1^2 + u_2^2 + \cdots + u_m^2}{m-1}} \tag{10}$$

In this research, Wyko NT 8000 is used to measure the surface roughness value, whose resolution is down to 0.16 nm. For the machined surface at different cutting distances, 100 samples are measured to calculate the peak-to-valley roughness, the measured data are then processed based on Eq. (10), and the processed peak-to-valley values of the machined surface at each cutting distance are listed in Table 2.

From Table 2, it is found that the mean value of the peak-to-valley (p–v) surface roughness increases slightly with the growing up of the cutting distance. As the cutting distance increases from 1000 to 5000 m, the mean value of p–v surface roughness increases from 123.7 to 125.5 nm correspondingly; the increase of the mean p–v value is about 2 nm. However, it is found from Table 2 that the standard deviation of the p–v value for each cutting distance is about 10 nm; therefore, this leads to the uncertainty of the surface roughness increase due to the larger standard deviation than the increase of the mean p–v value. Since other surface-influencing factors such as tool vibration and background noise exist throughout the cutting process, and the longer cutting distances lead to a relatively wider wear land of cutting tools, the increasing surface roughness is attributed to the effect of tool flank wear caused by the plowing effect and material springback.

4 Conclusions

Through an extensive cutting experiment, the tool wear characteristics at different tool wear stages in ultra-precision fly cutting (UPFC) and their effects on cutting chip morphology, cutting force signals, and machined surface quality were investigated. Specific conclusions drawn from this experiment are as follows:

1. At the tool wear early stage, the tool wear characteristics tend to be fractures of the cutting edge. These fractures occur on the cutting edge and follow statistical laws. The occurrence of tool fracture wear is imprinted both on the cutting chips and machined surface as a group of ridges.
2. Material welding on the rake face is another wear pattern of a diamond tool. Material welding can enlarge the cutting force in the thrust direction and decentralize the power spectrum density of the cutting force. In addition, material welding can lead to the breakage of cutting chips, which deteriorates the machined surface quality by scratching it and making it fuzzy and burred.
3. A wear land is formed at the steady tool wear stage. The width of the wear land increases with the increasing cutting distance. The formation of the wear land can make the cutting chips form a shutter-like structure at the tool entry side and increase the peak-to-valley roughness of the machined surface.
4. The formation of sub-wear land is another tool wear pattern in UPFC. The sub-wear land can reduce the wear land angle and re-sharpen the cutting edge.
5. Tool wear characteristics in UPFC also occur as micro-grooves on the flank face of cutting tools. The micro-grooves leave traces on the machined surface.

Acknowledgments The work described in this paper was partially supported by a grant from the National Natural Science Foundation of China (NSFC) (Project No.: 51275434) and the Research Grants Council of the Hong Kong Special Administrative Region, People's Republic of China (Project No.: PolyU 528710).

References

1. Yen YC, Söhner J, Lilly B, Altan T (2004) Estimation of tool wear in orthogonal cutting using the finite element analysis. J Mater Process Technol 146(1):82–91
2. Liu ZQ, Ai X, Zhang H, Wang ZT, Wan Y (2002) Wear patterns and mechanisms of cutting tools in high-speed face milling. J Mater Process Technol 129(1–3):222–226
3. Jawaid A, Che-Haron CH, Abdullah A (1999) Tool wear characteristics in turning of titanium alloy Ti-6246. J Mater Process Technol 92–93:329–334
4. Luo SY, Liao YS, Tsai YY (1999) Wear characteristics in turning high hardness alloy steel by ceramic and CBN tools. J Mater Process Technol 88:114–121
5. Zhang Z, Yan J, Kuriyagawa T (2011) Study on tool wear characteristics in diamond turning of reaction-bonded silicon carbide. Int J Adv Manuf Technol 57(1–4):117–125
6. Sharif Uddin M, Seah KHW, Li XP, Rahman M, Liu K (2004) Effect of crystallographic orientation on wear of diamond tools for nano-scale ductile cutting of silicon. Wear 257(7–8):751–759
7. Wadaa R, Kodamaa H, Nakamuraa K, Mizutanib Y, Shimurab Y, Takenakac N (1980) Wear characteristics of single crystal diamond tool. CIRP Ann Manuf Technol 29(1):47–52
8. Bakkal M, Shih Albert J, Scattergood Ronald O (2004) Chip formation, cutting forces, and tool wear in turning of Zr-based bulk metallic glass. Int J Mach Tools Manuf 44(9):915–925
9. Jia P, Zhou M (2012) Tool wear and its effect on surface roughness in diamond cutting of glass soda-lime. Chin J Mech Eng 25(6): 1224–1230

10. Pavel R, Marinescu I, Deis M, Pillar J (2005) Effect of tool wear on surface finish for a case of continuous and interrupted hard turning. J Mater Process Technol 170(1):341–349
11. Nastanka VOONM, Orodja OIV (2012) The influence of tool wear on the chip-forming mechanism and tool vibrations. Mater Tehnol 46(3):279–285
12. Meena A, El Mansori M (2013) Specific cutting force, tool wear and chip morphology characteristics during dry drilling of austempered ductile iron (ADI). Int J Adv Manuf Technol 69(9–12):2833–2841
13. Katuku K, Koursaris A, Sigalas I (2009) Wear, cutting forces and chip characteristics when dry turning ASTM grade 2 austempered ductile iron with PcBN cutting tools under finishing conditions. J Mater Process Technol 209(5):2412–2420
14. Huang Y, Liang SY (2005) Modeling of cutting forces under hard turning conditions considering tool wear effect. J Manuf Sci Eng 127(2):262–270
15. Zhang G, To S, Xiao G (2014) A novel spindle inclination error identification and compensation method in ultra-precision raster milling. Int J Mach Tools Manuf 78:8–17
16. To S, Zhang G (2014) Study of cutting force in ultra-precision raster milling of V-groove. Int J Adv Manuf Technol 75(5–8):967–978
17. Zuiker C, Krauss AR, Gruen DM (1995) Physical and tribological properties of diamond films grown in argoncarbon plasmas. Thin Solid Films 270(1):154–159
18. Song YC, Nezu K, Park CH, Moriwaki T (2009) Tool wear control in single-crystal diamond cutting of steel by using the ultra-intermittent cutting method. Int J Mach Tools Manuf 49(3–4): 339–343
19. Yin ZQ, To S, Lee WB (2009) Wear characteristics of diamond tool in ultra-precision raster milling. Int J Adv Manuf Technol 44(7–8): 638–647
20. Zhang G, To S, Xiao G (2014) Novel tool wear monitoring method in ultra-precision raster milling using cutting chips. Precis Eng 38(3):555–560
21. Zhang G, To S, Xiao G (2014) The relation between chip morphology and tool wear in ultra-precision raster milling. Int J Mach Tools Manuf 80–81:11–17
22. Arcona C, Dow Th A (1998) An empirical tool force model for precision machining. J Manuf Sci Eng 120(4):700–707
23. Kang IS, Kim JS, Kim JH, Kang MC, Seo YW (2007) A mechanistic model of cutting force in the micro end milling process. J Mater Process Technol 187–188:250–255
24. Drescher JD (1992) Tool force, tool edge and surface finish relationships in diamond turning. PhD Dissertation, North Carolina State University
25. Sze YK, Lee WB, Cheung CF, To S (2006) A power spectrum analysis of effect of rolling texture on cutting forces in single-point diamond turning. J Mater Process Technol 180(1–3):305–309